Electromagnetic propagation into reinforced-concrete walls

Elodie Richalot, Matthieu Bonilla, Wong Man-Fai, Victor Fouad Hanna, Henri Baudrand, Wiart Joe

Electromagnetic Propagation into Reinforced-Concrete Walls

Elodie Richalot, Matthieu Bonilla, Man-Faï Wong, *Senior Member, IEEE*, Victor Fouad-Hanna, *Fellow, IEEE*, Henri Baudrand, *Senior Member, IEEE*, and Joe Wiart, *Member, IEEE*

***Abstract*—A rigorous method for analyzing building construction materials, using finite-element techniques and an expansion of fields in Floquet's modes, is exposed in this paper. It allows us to precisely study the electromagnetic properties of buildings walls in terms of transmission and reflection characteristics, which can be useful in the design of wireless communication systems. First, we present the influence of the wall's parameters, namely, its thickness, the square side length, and the steel diameter of a concrete grid. The influence of the angle of arrival of the incident wave and the effect of considering the diffused field on the electromagnetic properties are then presented.**

***Index Terms*—Electromagnetic propagation, finite-element method, Floquet modes, mobile communication.**

I. Introduction

TO EVALUATE the quality of a wireless communication network, operators need tools to predict urban and indoor propagation. Ray-tracing models are widely used in determining electromagnetic properties of the radio channel. To develop this method, the knowledge of transmission and reflection characteristics of the construction materials are necessary. In modern buildings, two types of walls are commonly employed, namely, concrete walls and reinforced concrete ones, which are typically made up of a steel grid embedded in a slab of concrete. When using the ray-tracing method, multipath reflections and transmissions in concrete slabs are usually modeled by Fresnel coefficients, which is a rough approximation of the propagation. To get accurate propagation prediction, it is essential to precisely determine the transmission and reflection coefficients of the material involved, and this is the aim of the method presented here to enable the development of the ray-tracing technique by obtaining the necessary coefficients. It is particularly important to compare the electromagnetic performance of concrete walls and reinforced concrete walls to evaluate the influence of the steel grid. From the other hand, when using simpler models, coefficients independent of the direction of arrival have to also be derived in terms of diffuse fields.

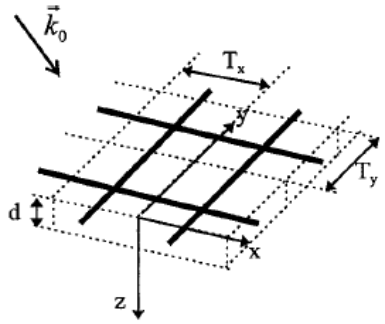

Fig. 1. Infinite reinforced concrete wall.

Two trends are generally adopted when studying metallic grids. The first one is based on the use of approximate formulas and is only available for concrete mesh dimensions, which are small compared to the wavelength [1]. The second one is based on the use of rigorous numerical methods. The method of moment was successively employed in the study of grids of any geometry [2]. However, this last method is less suited to study complex grids inserted into lossy multilayers. Thus, we have chosen to use the finite-element method (FEM) because this rigorous method presents the advantage of being able to take into account complex geometries and inhomogeneities. Two frequencies of operation, i.e., 900 and 1800 MHz, are chosen due to the importance of the results for indoor and outdoor wireless communications.

II. Theory

A. Elementary Cell

A reinforced concrete wall is modeled as an infinite biperiodic multilayer structure. The dimensions of the wall are considered large enough compared to the wavelength. The wall is composed of a square grid immersed in a dielectric slab. More layers, corresponding to more complex materials, can also be considered. The studied structure is a reinforced concrete wall illuminated by a plane wave of wave vector $\vec{k}_0 = {}^t(k_x, k_y, k_z)$, as shown in Fig. 1.

According to Floquet's theorem, periodic boundary conditions involve the periodicity of the fields, which follow the relations [3]:

$$f(x + T_x, y, z) = f(x, y, z)e^{-jk_x T_x}$$

and

$$f(x, y + T_y, z) = f(x, y, z)e^{-jk_y T_y} \quad (1)$$

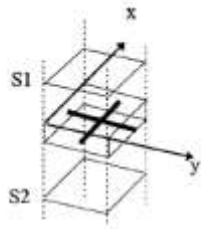

Fig. 2. Elementary cell.

for a $e^{j\omega t}$ time dependency, where T_x and T_y are the geometrical structure period. This allows us to reduce the studied domain to an elementary cell by employing (1) as a boundary condition on the lateral sides of the cell (Fig. 2).

B. Decomposition on Floquet's Harmonics

The resolution of the Helmholtz equation having periodic boundary conditions in the $z = 0$ plane leads to a solution that can be written as the sum of an infinite discrete expansion of plane waves that are called Floquet's modes. These plane waves are orthogonal and their wave vectors $\vec{k}_{mn} = {}^t(k_{xmn}, k_{ymn}, \pm k_{zmn})$ are functions of the incident wave [3]

$$\begin{aligned} k_{xmn} &= k_x + \frac{2\pi m}{T_x} \\ k_{ymn} &= k_y + \frac{2\pi n}{T_y} \\ k_{zmn}^2 &= k_0^2 - k_{xmn}^2 - k_{ymn}^2. \end{aligned} \tag{2}$$

Once these plane waves have been decomposed into TE and TM waves, it is possible to express the tangential fields to define a complete and orthogonal set of TE and TM plane wave as follows:

$$\begin{aligned} \vec{e}_{\mathrm{TE}mn_{(x,y)}} &= Z_{\mathrm{TE}mn}^{1/2} \frac{(-k_{ymn}\vec{x} + k_{xmn}\vec{y})}{k_{tmn} \cdot \sqrt{S_1}} e^{-j(k_{xmn}x + k_{ymn}y)} \\ \vec{h}_{\mathrm{TE}mn_{(x,y)}} &= Y_{\mathrm{TE}mn}\left(-\vec{z} \times \vec{e}_{\mathrm{TE}mn_{(x,y)}}\right) \end{aligned} \tag{3}$$

$$\begin{aligned} \vec{e}_{\mathrm{TM}mn_{(x,y)}} &= Z_{\mathrm{TM}mn}^{1/2} \frac{(k_{xmn}\vec{x} + k_{ymn}\vec{y})}{k_{tmn} \cdot \sqrt{S_1}} e^{-j(k_{xmn}x + k_{ymn}y)} \\ \vec{h}_{\mathrm{TM}mn_{(x,y)}} &= Y_{\mathrm{TM}mn}\left(-\vec{z} \times \vec{e}_{\mathrm{TM}mn_{(x,y)}}\right) \end{aligned} \tag{4}$$

where

$$\begin{aligned} Z_{\mathrm{TE}mn} &= \frac{\omega\mu}{k_{zmn}} \\ Z_{\mathrm{TM}mn} &= \frac{k_{zmn}}{\omega\varepsilon} \end{aligned}$$

and

$$k_{tmn}^2 = k_{xmn}^2 + k_{ymn}^2 \tag{5}$$

with the orthogonality relations

$$\begin{aligned} &\int_0^T \int_0^T \left(\vec{e}_{\mathrm{TE}mn} \times \vec{h}_{\mathrm{TE}m'n'}\right) \cdot \vec{z}\, dx\, dy = 0, \\ &\text{for } (m, n) \neq (m', n') \end{aligned} \tag{6}$$

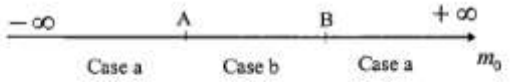

Fig. 3. Different cases for m_0.

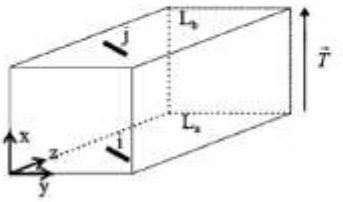

Fig. 4. Elementary cell and opposite sidewalls.

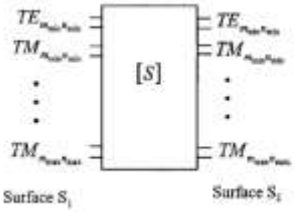

Fig. 5. Network representation of the problem.

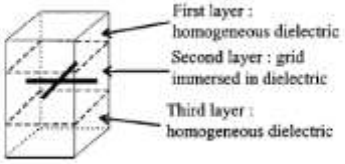

Fig. 6. Reinforced-concrete wall decomposed into three cascaded layers.

$$\begin{aligned} &\int_0^T \int_0^T \left(\vec{e}_{\mathrm{TM}mn} \times \vec{h}_{\mathrm{TM}m'n'}\right) \cdot \vec{z}\, dx\, dy = 0, \\ &\text{for } (m, n) \neq (m', n') \end{aligned} \tag{7}$$

and normalized as

$$\begin{aligned} \int_0^T \int_0^T \|\vec{e}_{\mathrm{TE}mn}\|^2\, dx\, dy &= |Z_{\mathrm{TE}mn}| \\ \int_0^T \int_0^T \|\vec{e}_{\mathrm{TM}mn}\|^2\, dx\, dy &= |Z_{\mathrm{TM}mn}|. \end{aligned} \tag{8}$$

For the problem exposed in Fig. 1, fields can be written as follows.

For $z < 0$

$$\begin{aligned} \vec{E}_{(x,y,z)} = {} & a'_{00} e^{-jk_{z00}z} \vec{e}_{\mathrm{TE}00}(x, y) + a''_{mn} e^{-jk_{zmn}z} \vec{e}_{\mathrm{TM}00}(x, y) \\ & + \sum_{m=-\infty}^{+\infty} \sum_{n=-\infty}^{+\infty} \left[b'_{mn} e^{jk_{zmn}z} \vec{e}_{\mathrm{TE}_{mn}}(x, y) \right. \\ & \left. + b''_{mn} e^{jk_{zmn}z} \vec{e}_{\mathrm{TM}_{mn}}(x, y)\right] \end{aligned} \tag{9}$$

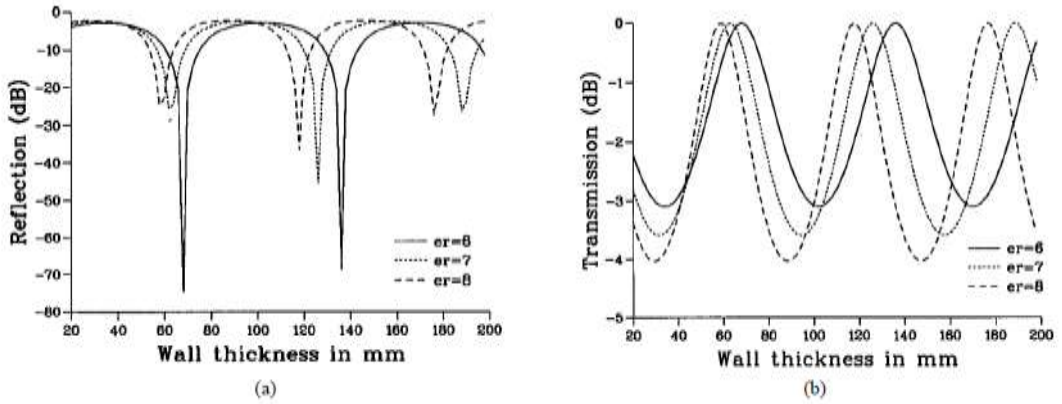

Fig. 7. Reflection and transmission coefficients for walls of relative permittivity of 6, 7, or 8.

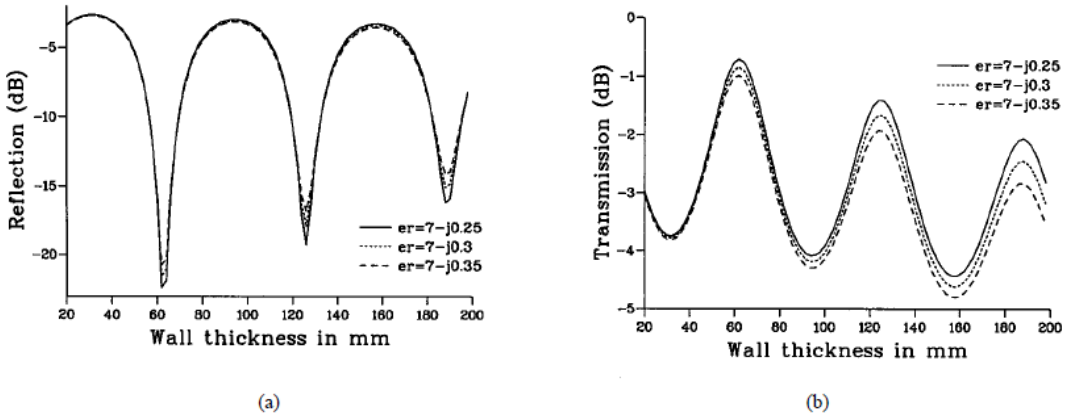

Fig. 8. Reflection and transmission for walls of relative permittivity of $(7 - j0 \cdot 25)$, $(7 - j0 \cdot 3)$, and $(7 - j0 \cdot 35)$.

and

$$\vec{H}_{(x,y,z)} = c'_{00}\, e^{-jk_{z00}z}\vec{h}_{TE_{00}(x,y)} + c''_{mn}\, e^{-jk_{zmn}z}\vec{h}_{TM_{00}(x,y)} - \sum_{m=-\infty}^{+\infty}\sum_{n=-\infty}^{+\infty}\left[b'_{mn}\, e^{jk_{zmn}z}\vec{h}_{TE_{mn}(x,y)} + b''_{mn}\, e^{jk_{zmn}z}\vec{h}_{TM_{mn}(x,y)}\right]. \tag{10}$$

For $z > d$

$$\vec{E}_{(x,y,z)} = \sum_{m=-\infty}^{+\infty}\sum_{n=-\infty}^{+\infty}\left[c'_{mn}\, e^{-jk_{zmn}z}\vec{e}_{TE_{mn}(x,y)} + c''_{mn}\, e^{-jk_{zmn}z}\vec{e}_{TM_{mn}(x,y)}\right] \tag{11}$$

$$\vec{H}_{(x,y,z)} = \sum_{m=-\infty}^{+\infty}\sum_{n=-\infty}^{+\infty}\left[c'_{mn}\, e^{-jk_{zmn}z}\vec{h}_{TE_{mn}(x,y)} + c''_{mn}\, e^{-jk_{zmn}z}\vec{h}_{TM_{mn}(x,y)}\right]. \tag{12}$$

The number of modes in the decomposition of the fields is infinite, but for large values of $|m|$ and $|n|$, the modes are evanescent. Therefore, we can truncate the expansion, e.g., the m index to m_0. The $\mathrm{TE}_{m_0 n}$ and $\mathrm{TM}_{m_0 n}$ modes are propagative for $k^2_{zm_0 n} > 0$. We have to consider the following two cases depending on m_0 (Fig. 3).

- *Case a*: $m_0 \leq A$ or $m_0 \geq B$ with $A = -(T_u/2\pi)(k_0 + k_x)$ and $B = (T_u/2\pi)(k_0 - k_x)$. All the $\mathrm{TE}_{m_0 n}$ and $\mathrm{TM}_{m_0 n}$ modes are evanescent.
- *Case b*: $A < m_0 < B$: Floquet's modes are propagative for $N1 < n < N2$ with

$$N_1 = \frac{-\sqrt{k_0^2 - \left(k_x + \frac{2\pi}{T}m_0\right)^2} - k_y}{\frac{2\pi}{T}}$$

and

$$N_2 = \frac{\sqrt{k_0^2 - \left(k_x + \frac{2\pi}{T_u}m_0\right)^2} - k_y}{\frac{2\pi}{T}}. \tag{13}$$

Thus, in certain conditions, there are propagative modes in non-specular directions. Their influence will be discussed later.

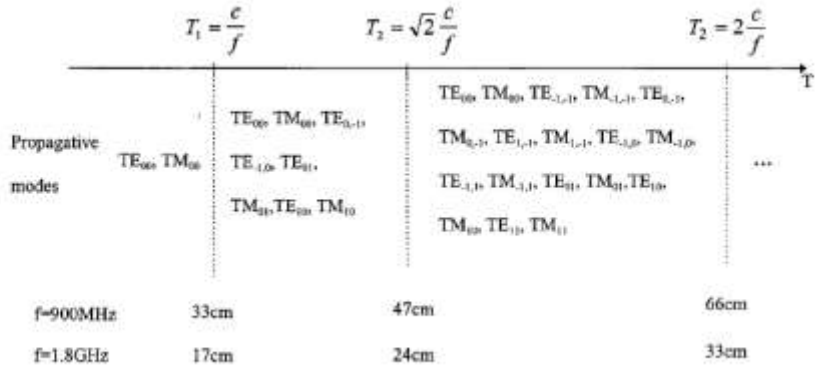

Fig. 9. Propagative modes in normal incidence at 900 MHz and 1.8 GHz for a grid of period T.

C. The FEM

The E-field variational formulation of the electromagnetic problem of a domain having a volume Ω can be written in the form

$$\int_\Omega \frac{1}{\mu_r}\mathrm{curl}\vec{E}\cdot\mathrm{curl}\vec{E}'\,dv - k^2\int_\Omega \varepsilon_r\vec{E}\cdot\vec{E}'\,dv = j\omega\mu_0\int_{\partial\Omega}\left(\vec{H}\times\vec{n}\right)\cdot\vec{E}'\,ds \quad (14)$$

where $\partial\Omega$ represents the boundary of the domain Ω, which has to be verified for each test function $\vec{E}'$. In our FEM formulation, the domain to be studied is decomposed into tetrahedral elements, and the electric field is decomposed on edge elements [4]

$$\vec{E} = \sum_{\text{edges}\ a} e_a\vec{w}_a \quad (15)$$

where $\vec{w}_a$ are edge elements and the degrees of freedom e_a are the circulation of the electric field on the associated edges. The Galerkin procedure leads to the following relation:

$$\forall m,\ \sum_n e_n\int_\Omega\left[\frac{1}{\mu_r}\mathrm{curl}\vec{w}_m\cdot\mathrm{curl}\vec{w}_n - k^2\varepsilon_r\vec{w}_m\cdot\vec{w}_n\right]dv = j\omega\mu_0\int_{\partial\Omega}\left(\vec{H}\times\vec{n}\right)\cdot\vec{w}_m\,ds \quad (16)$$

which can be written in a matrix form as a sparse linear system

$$[G](e) = j\omega\mu_0(J) \quad (17)$$

where the vector (e) contains the degrees of freedom e_a on the edges, and (J) describes the Neuman-type boundary conditions given by

$$J_m = \int_{\partial\Omega}\left(\vec{H}\times\vec{n}\right)\cdot\vec{w}_m\,ds \quad (18)$$

where $\vec{n}$ is the normal vector entering the domain Ω.

The studied domain Ω has to be bounded. We already have defined the lateral sides of the cell, at which periodicity conditions are applied. To simply express the boundary conditions on the sidewalls of the elementary cell, the mesh is created in such away that meshes on opposite surfaces are identical. Thus, by translating this elementary cell with respect to $kT_x\hat{x}$ and $kT_y\hat{y}$,

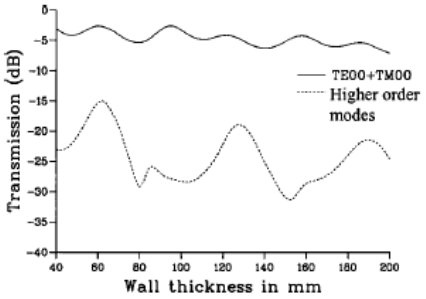

Fig. 10. Influence of higher order modes for a grid of 25-cm square length for a normal incidence at 1.8 GHz.

the infinite array is reconstructed with conforming meshes between interfaces. Let us consider the elementary cell with opposite periodic surfaces L_a and L_b (Fig. 4).

Equation (17) has lines corresponding to the degrees of freedom located on the sidewalls, e.g., those involving edge i on L_a and edge j on L_b. The currents J_i and J_j must be known to solve (17). As j corresponds to i by the translation vector $\vec{T}$, the periodicity condition gives the relations

$$J_j = -e^{-j\vec{k}\cdot\vec{T}}\,J_i \quad (19)$$

$$e_j = e^{-j\vec{k}\cdot\vec{T}}\,e_i. \quad (20)$$

Inserting these conditions in the linear system given by (17), it can be seen that degrees of freedom like j can be expressed only as a function of the degrees of freedom like i. This can be interpreted as if L_a and L_b are merged, recreating an infinite mesh by wrapping opposite side walls onto each other.

D. Network Representation

As fields in free space are written as expansions on Floquet's modes, free space can be considered as a waveguide whose eigenmodes are Floquet's harmonics. We saw that these modes are orthogonal, propagative, or evanescent, exactly as in conventional waveguides. The wave propagation in the direction of the incident wave before and after the walls can be represented by

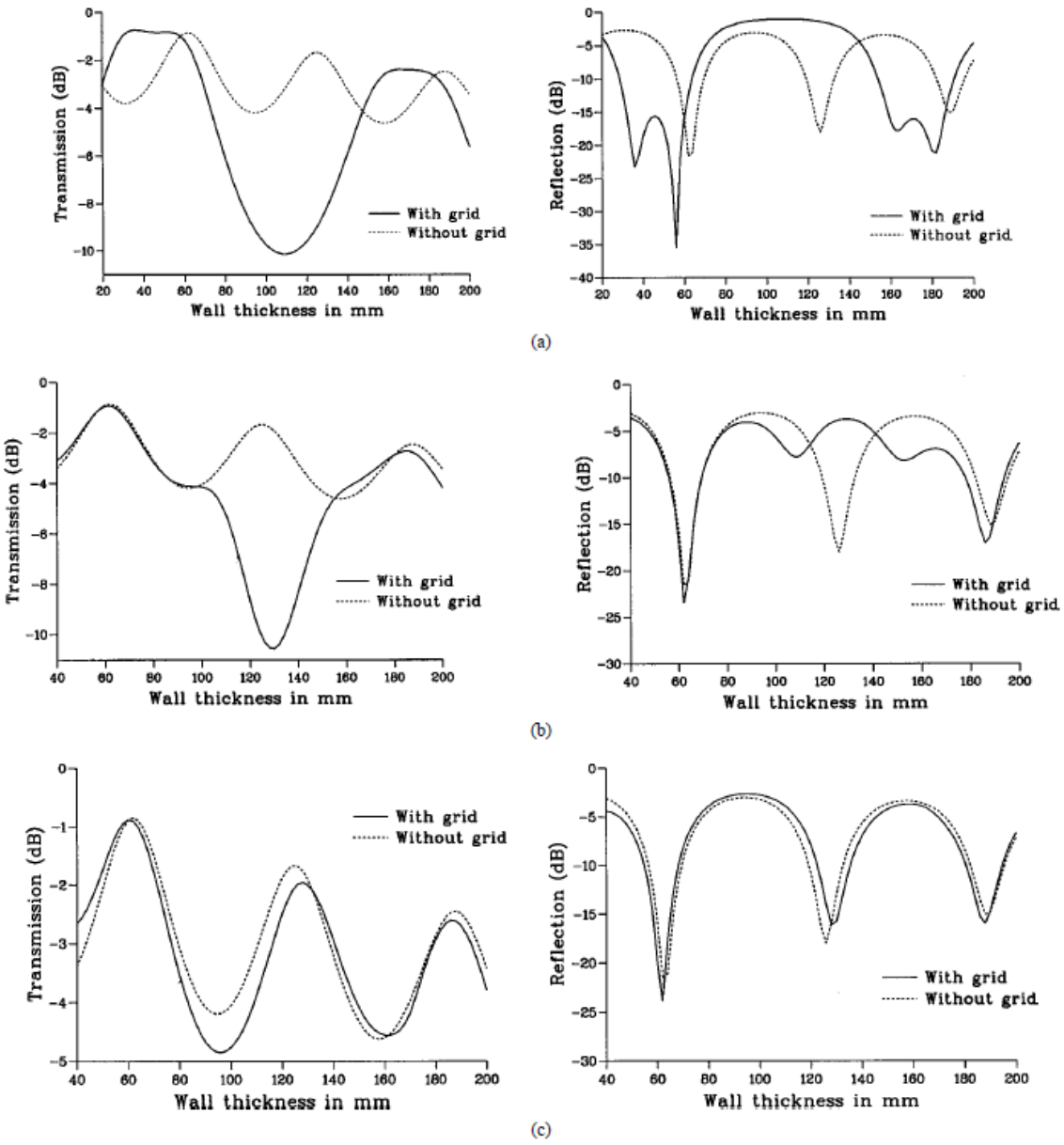

Fig. 11. Transmission and reflection at 900 MHz for a normal incidence for a grid having a square side length of: (a) 5, (b) 15, and (c) 25 cm.

a network whose ports are excited by Floquet modes [4]. Fig. 5 shows the corresponding scheme.

In order to determine the scattering matrix for this network, we calculate the impedance matrix by imposing magnetic fields on the ports. The resolution of a sparse system leads to the determination of fields for each excitation. The impedance matrix is then determined as follows: when the port i on surface S_1 or S_2 (Fig. 2) is excited by the normalized magnetic field $\vec{h}_i$ of the associated Floquet's mode, and all others ports are open circuited, the resolution of the system gives the electric field $\vec{E}^{(i)}$ in the whole domain Ω. We have for each port j

$$Z_{ij} = \int_{S_1+S_2} \left(\vec{h}_j \times \vec{n}\right) \cdot \vec{E}^{(i)}\, ds. \tag{21}$$

Fields are expressed in terms of voltages and currents on the surfaces S_1 and S_2 as

$$\vec{E}_{(x,y,z)} = \sum_{m=m_{\min}}^{m_{\max}} \sum_{n=n_{\min}}^{n_{\max}} \left[V^{I}_{mn}\vec{e}_{\mathrm{TE}_{mn}}(x,y) + V^{II}_{mn}\vec{e}_{\mathrm{TM}_{mn}}(x,y)\right] \tag{22}$$

$$\vec{H}_{(x,y,z)} = \sum_{m=m_{\min}}^{m_{\max}} \sum_{n=n_{\min}}^{n_{\max}} \left[I^{I}_{mn}\vec{h}_{\mathrm{TE}_{mn}}(x,y) + I^{II}_{mn}\vec{h}_{\mathrm{TM}_{mn}}(x,y)\right] \tag{23}$$

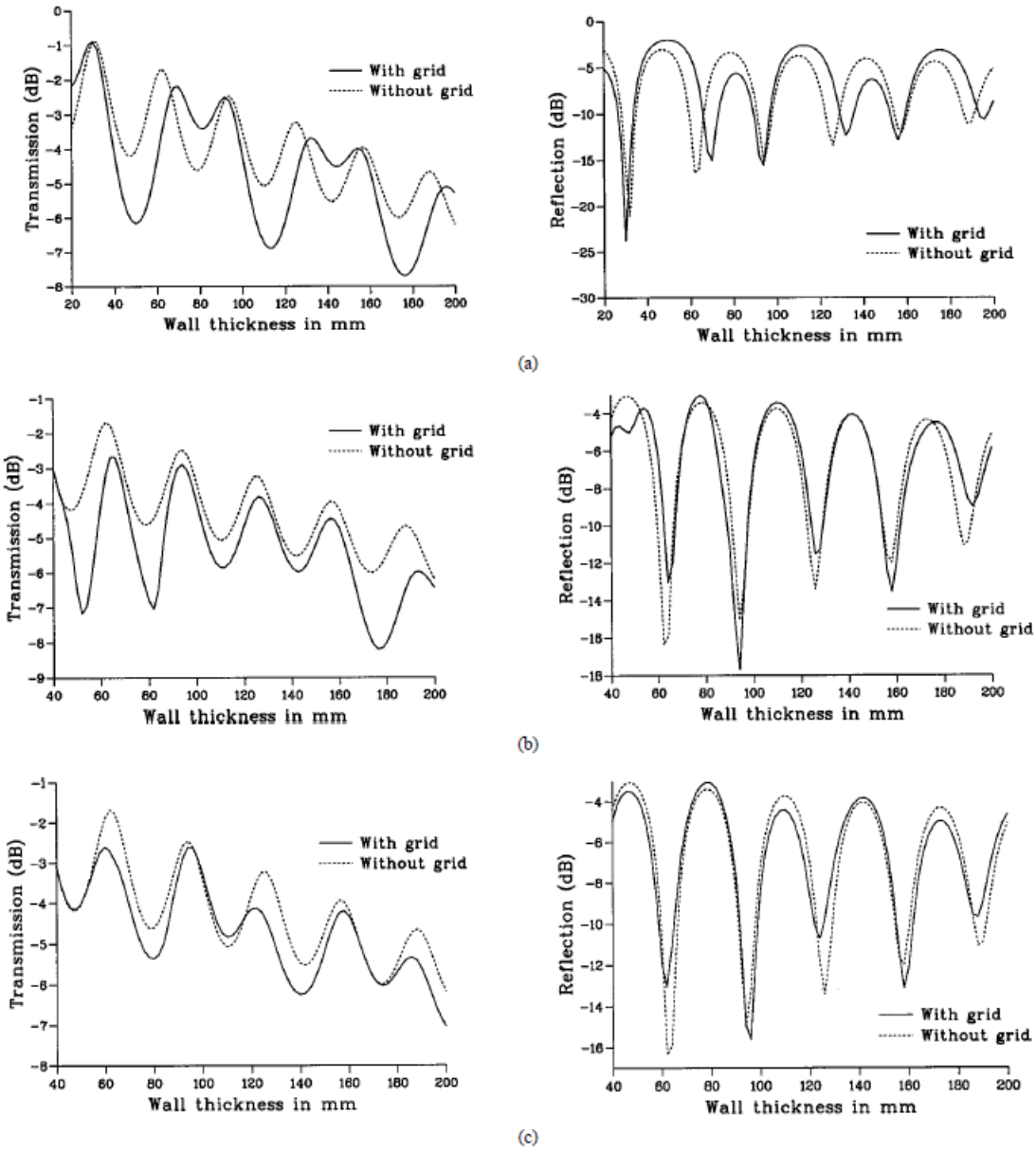

Fig. 12. Transmission and reflection at 1.8 GHz for a normal incidence with a grid having square side length of: (a) 5, (b) 15, and (c) 25 cm.

with (24), shown at the bottom of this page, and (25), shown at the bottom of the following page, we find the relation between the impedance and admittance matrices

$$[S] = ([Z] + [I])^{-1}([Z] - [I]) \tag{26}$$

where $[I]$ is the unit matrix.

The calculated scattering matrix contains all the information about the transmission and reflection properties of the structure for the chosen incident field. We can then find the reflection and transmission coefficients.

E. Cascade Connection of Layers

The studied structure can be seen as composed of three cascaded biperiodic layers: the first and third are layers of homo-

$$\vec{E}_{(x,y,z)} = \sum_{m=m_{\min}}^{m_{\max}} \sum_{n=n_{\min}}^{n_{\max}} \left[\left(a'_{mn}\, e^{-jk_{zmn}z} + b'_{mn}\, e^{jk_{zmn}z} \right) \vec{e}_{\mathrm{TE}_{mn}(x,y)} + \left(a''_{mn}\, e^{-jk_{zmn}z} + b''_{mn}\, e^{jk_{zmn}z} \right) \vec{e}_{\mathrm{TM}_{mn}(x,y)} \right] \tag{24}$$

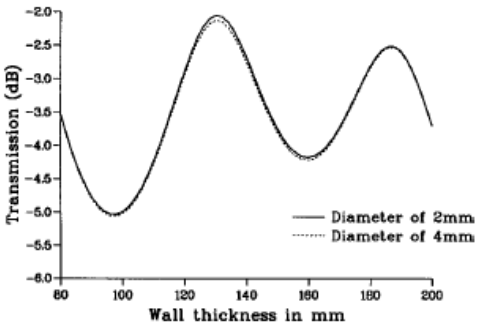

Fig. 13. At 900 MHz.

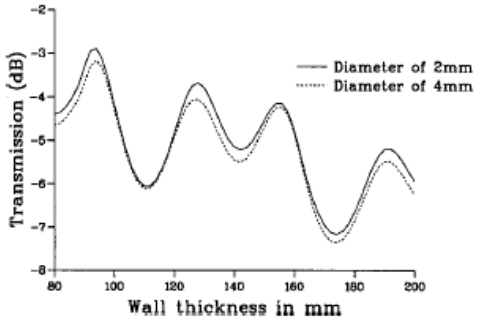

Fig. 14. At 1.8 GHz.

geneous dielectric, the second is composed of a square grid immersed in a dielectric (Fig. 6). It is interesting to study them separately in order to reduce the volume of the domain treated by the FEM. If two layers are characterized by their scattering matrices S_1 and S_2, the scattering matrix of the two cascaded layers is given by

$$[S] = \begin{pmatrix} \overline{S}^1_{11} & 0 \\ \overline{S}^2_{21} \cdot \overline{S}^1_{21} & \overline{S}^2_{22} \end{pmatrix} + \begin{pmatrix} \overline{S}^1_{12} \\ \overline{S}^2_{21} \cdot \overline{S}^1_{22} \end{pmatrix} \cdot \left(1 - \overline{S}^2_{11} \cdot \overline{S}^1_{22}\right)^{-1} \begin{pmatrix} \overline{S}^2_{11} \cdot \overline{S}^1_{21} & \overline{S}^2_{12} \end{pmatrix} \quad (27)$$

where the involved blocks are given by

$$[S_1] = \begin{pmatrix} \overline{S}^1_{11} & \overline{S}^1_{12} \\ \overline{S}^1_{21} & \overline{S}^1_{22} \end{pmatrix}$$
$$[S_2] = \begin{pmatrix} \overline{S}^2_{11} & \overline{S}^2_{12} \\ \overline{S}^2_{21} & \overline{S}^2_{22} \end{pmatrix}. \quad (28)$$

Furthermore, the wall is composed of homogeneous dielectric layers whose scattering matrices can be determined analytically. The scattering matrix of a dielectric layer of dielectric constant ε_r and thickness l is diagonal by block. Each block corresponds

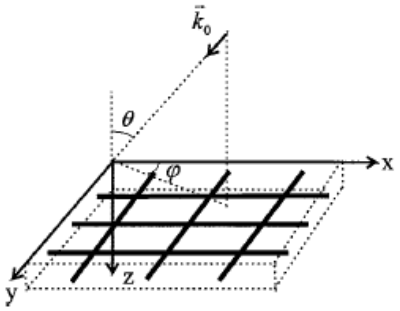

Fig. 15. Problem geometry.

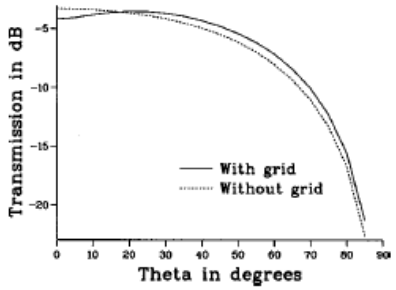

Fig. 16. $\varphi = 0$ (polarization TE).

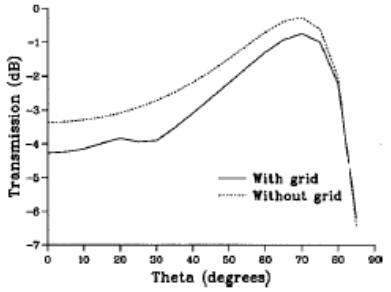

Fig. 17. $\varphi = 0$ (polarization TM).

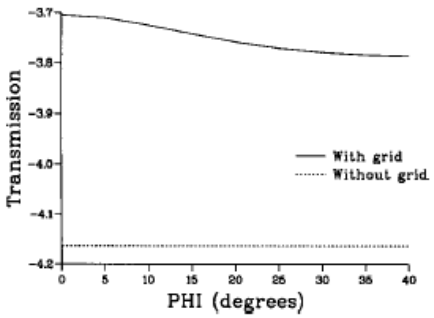

Fig. 18. $\theta = \pi/6$ (polarization TE).

$$\vec{H}_{(x,y,z)} = \sum_{m=m_{\min}}^{m_{\max}} \sum_{n=n_{\min}}^{n_{\max}} \left[\left(a'_{mn}\, e^{-j k_{zmn} z} - b'_{mn}\, e^{j k_{zmn} z}\right) \vec{h}_{\mathrm{TE}_{mn}}(x,y) + \left(a''_{mn}\, e^{-j k_{zmn} z} - b''_{mn}\, e^{j k_{zmn} z}\right) \vec{h}_{\mathrm{TM}_{mn}}(x,y) \right] \quad (25)$$

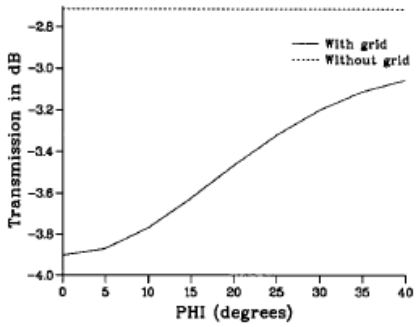

Fig. 19. $\theta = \pi/6$ (polarization TM).

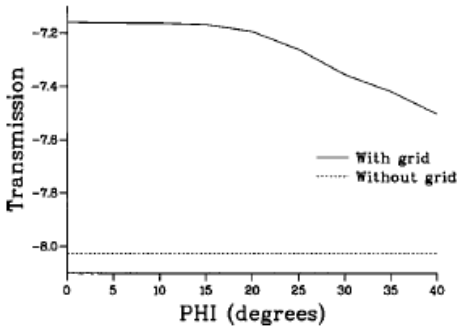

Fig. 20. $\theta = \pi/3$ (polarization TE).

to one TE or TM Floquet's mode and is, for the TE_{mn} or the TM_{mn} modes

$$\overline{S}_{mn} = \begin{pmatrix} 0 & e^{-jk_{zmn}^{\varepsilon_r} l} \\ e^{-jk_{zmn}^{\varepsilon_r} l} & 0 \end{pmatrix}$$

with

$$k_{zmn}^{\varepsilon_r} = \left(k_0^2 \varepsilon_r - k_{xmn}^2 - k_{ymn}^2\right)^{1/2}, \tag{29}$$

The interface between two dielectric layers of dielectric constants ε_{r_1} and ε_{r_2} is also defined by a scattering matrix diagonal by block, and we have for the TE_{mn} mode

$$\overline{S}_{\mathrm{TE}_{mn}} = \begin{pmatrix} \dfrac{k_{zmn}^{\varepsilon_{r_1}} - k_{zmn}^{\varepsilon_{r_2}}}{k_{zmn}^{\varepsilon_{r_1}} + k_{zmn}^{\varepsilon_{r_2}}} & \dfrac{2\left(k_{zmn}^{\varepsilon_{r_1}} k_{zmn}^{\varepsilon_{r_2}}\right)^{1/2}}{k_{zmn}^{\varepsilon_{r_1}} + k_{zmn}^{\varepsilon_{r_2}}} \\ \dfrac{2\left(k_{zmn}^{\varepsilon_{r_1}} k_{zmn}^{\varepsilon_{r_2}}\right)^{1/2}}{k_{zmn}^{\varepsilon_{r_1}} + k_{zmn}^{\varepsilon_{r_2}}} & \dfrac{-k_{zmn}^{\varepsilon_{r_1}} + k_{zmn}^{\varepsilon_{r_2}}}{k_{zmn}^{\varepsilon_{r_1}} + k_{zmn}^{\varepsilon_{r_2}}} \end{pmatrix} \tag{30}$$

and for the TM_{mn} mode

$$\overline{S}_{\mathrm{TM}_{mn}} = \begin{pmatrix} \dfrac{\dfrac{\varepsilon_{r_1}}{k_{zmn}^{\varepsilon_{r_1}}} - \dfrac{\varepsilon_{r_2}}{k_{zmn}^{\varepsilon_{r_2}}}}{\dfrac{\varepsilon_{r_1}}{k_{zmn}^{\varepsilon_{r_1}}} + \dfrac{\varepsilon_{r_2}}{k_{zmn}^{\varepsilon_{r_2}}}} & \dfrac{2\left(\dfrac{\varepsilon_{r_1}\varepsilon_{r_2}}{k_{zmn}^{\varepsilon_{r_1}} k_{zmn}^{\varepsilon_{r_2}}}\right)}{\dfrac{\varepsilon_{r_1}}{k_{zmn}^{\varepsilon_{r_1}}} + \dfrac{\varepsilon_{r_2}}{k_{zmn}^{\varepsilon_{r_2}}}} \\ \dfrac{2\left(\dfrac{\varepsilon_{r_1}\varepsilon_{r_2}}{k_{zmn}^{\varepsilon_{r_1}} k_{zmn}^{\varepsilon_{r_2}}}\right)}{\dfrac{\varepsilon_{r_1}}{k_{zmn}^{\varepsilon_{r_1}}} + \dfrac{\varepsilon_{r_2}}{k_{zmn}^{\varepsilon_{r_2}}}} & \dfrac{-\dfrac{\varepsilon_{r_1}}{k_{zmn}^{\varepsilon_{r_1}}} + \dfrac{\varepsilon_{r_2}}{k_{zmn}^{\varepsilon_{r_2}}}}{\dfrac{\varepsilon_{r_1}}{k_{zmn}^{\varepsilon_{r_1}}} + \dfrac{\varepsilon_{r_2}}{k_{zmn}^{\varepsilon_{r_2}}}} \end{pmatrix}. \tag{31}$$

These considerations considerably reduce the size of the computational system to be solved. Only the second layer is studied through numerical simulation and does not need any another treatment when the thickness of the wall is varied.

III. Results

A. Dielectric Characteristics

The knowledge of dielectric parameters of the wall is necessary to determine the transmission and reflection coefficients. These parameters vary with the material, environmental conditions (temperature, moisture content, etc.), and the frequency. Therefore, it is not easy to determine them precisely, and we have to know their influence on the results.

We can notice that the influence of a variation of 30% of the real part of the permittivity on the reflection and transmission coefficients is not negligible (Fig. 7). It increases with the increase of the wall thickness because of the variation of the propagation velocity within the wall. The dielectric losses are null

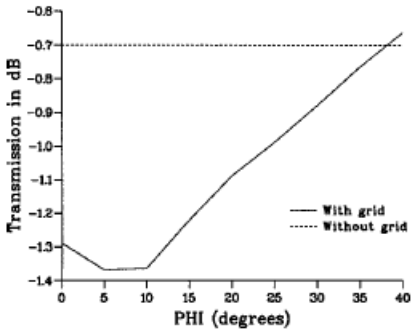

Fig. 21. $\theta = \pi/3$ (polarization TM).

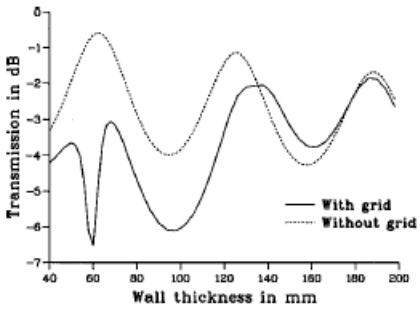

Fig. 22. Normal incidence.

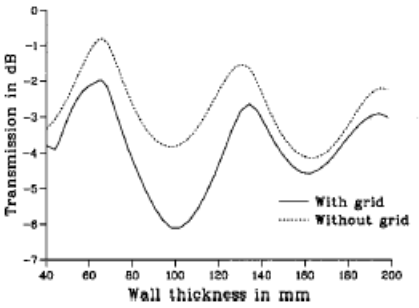

Fig. 23. Diffuse field.

TABLE I
TRANSMISSION SIMULATED AND MEASURED IN DIFFUSE FIELD

Frequency (GHz)	Transmission (dB) simulated	Transmission (dB) measured
1	-30.3	-30.1
5	-17.0	-14.9
10	-11.7	-11.0
15	-8.6	-9.6
20	-6.5	-9.6

for a real permittivity and increase with the imaginary part of the permittivity (Fig. 8).

B. Influence of Grid Dimensions

We have studied the influence of some critical parameters of the grid on the transmission characteristics of the wall and compared the results to those obtained for walls without grid.

1) Square Grid Side Length: To know the influence of the grid for usual square grid side length and wall thickness, we simulate walls for a mesh having a square side length varying from 5 to 25 cm, and for wall thickness varying from 20 to 200 mm. This study is made at 900 MHz and 1.8 GHz for a normal incidence and a relative permittivity $\varepsilon_r = 7 - j0 \cdot 3$. The steel diameter is 3 mm. As shown in Fig. 9, the number of propagative modes in free space increases as a function of the square side length.

For a periodicity of 25 cm, there are 16 propagative higher order modes at 1.8 GHz. Fig. 10 shows that their influence is negligible, as for all the other cases we deal with in this paper.

Transmission and reflection coefficients, as well as losses in the wall, are given in Figs. 11 and 12 for concrete with or without a grid. One can see that the influence of the presence of the grid cannot be neglected for the chosen dimensions.

2) Steel Diameter: For a relative permittivity $\varepsilon_r = 7 - j0 \cdot 3$ and a square grid of side length of 12 cm, steel diameters of 2 and 4 mm are considered. Results obtained at 900 MHz and 1.8 GHz are shown in Figs. 13 and 14. We can see that the influence of steel diameter variation has a negligible effect at 900 MHz, while at 1.8 GHz, the attenuation is more important when the diameter is bigger.

C. Diffuse Fields

Due to the multireflections phenomena involved in urban and indoor propagation, the electromagnetic fields have to be considered as the resultant of the incidence of a number of plane waves having different propagation directions and polarizations. Taking an infinite number of plane waves, this phenomena is well described by the concept of diffuse fields, for which each direction of propagation is equiprobable. This concept is more commonly known in a mode stirred chamber and can provide a good figure of merit on reflection or transmission characteristics when the incident field is not clearly known. As the mesh is square, the φ-angle sector can be restricted in the calculation, and the power transmission coefficients in diffuse fields are given by [5]

$$T_{\text{diffuse}} = \frac{2}{\pi} \int_0^{\pi/4} \int_0^{\pi/2} \left(T_{\text{TE}_{(\theta,\varphi)}} + T_{\text{TM}_{(\theta,\varphi)}} \right) \sin(2\theta)\, d\theta\, d\varphi$$

where T_{TE} and T_{TM} are the power coefficients for TE and TM polarized incident plane waves θ and φ angles define the incidence direction as defined in Fig. 15. To calculate the coefficients, we discretize the angle variation in $\pi/36$ and simulate the problem for each associated incidence.

The precision of our method has been verified for a steel grid of diameter 0.7 mm and mesh size 4.7 mm in the air. The results of our simulations are compared in Table I to measurements made in a stirring mode chamber [5]. Good agreement of the results can be noticed.

We have then studied a wall, whose square size length is 20 cm, steel diameter 8 mm, wall thickness 40 mm, and relative permittivity $\varepsilon_r = 7 - j0 \cdot 2$ at 900 MHz.

The influence of the direction of incidence of plane waves (Fig. 15) has first been studied in the plane $\varphi = 0$. Figs. 16 and 17 show that, in the TE-case, the transmission decreases when the incidence direction becomes oblique, as in the TM-case, the maximum of the transmission is not obtained for a normal incidence.

The influence of the variation of φ is then shown for $\theta = \pi/6$ (Figs. 18 and 19) and $\theta = \pi/3$ (Figs. 20 and 21).

The transmission properties as a function of wall thickness have been studied for the test case of normal incidence, and results are given in Fig. 22. Furthermore, this structure has been studied using a diffuse field concept, and results are shown in Fig. 23. It can be seen from these two figures that results are nearly identical for the case without grids, while, for the case of a wall with grids, the diffuse field concept gives different results. This is due to the presence of more reflections on the grids. The results also show that the presence of grids modifies the transmission properties of the walls.

IV. CONCLUSION

To study precisely reinforced-concrete walls, a method based on the FEM has been employed. Due to the biperiodicity of the studied structure, the studied domain was reduced to an elementary cell by the use of biperiodic boundary conditions, and fields in the open domain were decomposed on Floquet's harmonics.

The studied structure is entirely described by its associated scattering matrix of small dimensions. An extensive study of electromagnetic properties of reinforced-concrete walls showed that the dielectric permittivity has to be determined precisely, and that the influence of the grid cannot be neglected. It is shown that wall dimensions and the properties of incident field, mainly, its angle of incidence and the effect of considering it as a diffused one, have a nonnegligible effect on the transmission and reflection propagation properties into reinforced concrete walls.

REFERENCES

[1] J. R. Wait, "Theories of scattering from wire grids and mesh structures," in *Electromagnetic Scattering*. New York: Academic, 1978.

[2] R. Mittra, C. H. Chan, and T. Cwik, "Techniques for analyzing frequency selective surfaces—A review," *Proc. IEEE*, vol. 76, pp. 1593–1615, Dec. 1988.

[3] R. Petit, Ed., *Electromagnetic Theory of Gratings*. Berlin, Germany: Springer-Verlag, 1990.

[4] M. F. Wong, O. Picon, and V. Fouad-Hanna, "Three-dimensional finite element analysis of N-port waveguide junctions using edge-elements," *Int. J. Microwave Millimeter-Wave Computer-Aided Eng.*, vol. 3, no. 4, pp. 442–451, 1993.

[5] F. Gaudaire and Y. Gabillet, "Propagation radio dans le bâtiment: Une nouvell approche," *Rev. l'Elect. Electron.*, no. 11, Dec. 1997.